Organocatalytic Access to a cis-Cyclopentyl-γ-amino Acid: An Intriguing Model of Selectivity and Formation of a Stable 10/12-Helix from the Corresponding γ/α-Peptide.

Rossana Fanelli, Dénes Berta, Tamás Földes, Edina Rosta, Robert Andrew Atkinson, Hans-Jörg Hofmann, Kenneth Shankland, Alexander J A Cobb

Organocatalytic Access to a cis-Cyclopentyl-γ-amino Acid: An Intriguing Model of Selectivity and Formation of a Stable 10/12-Helix from the Corresponding γ/α-Peptide.

Rossana Fanelli,[†] Dénes Berta,[†] Tamás Földes,[†] Edina Rosta,[†] R. Andrew Atkinson,[‡] Hans-Jörg Hofmann,[¶] Kenneth Shankland,[§] and Alexander J. A. Cobb[*,†]

†*Department of Chemistry, King's College London, 7 Trinity Street, London SE1 1DB, UK*

‡*Randall Division of Cell and Molecular Biophysics, and the BHF Centre of Research Excellence, Centre for Biomolecular Spectroscopy, King's College London, London, UK*

¶*Institut für Biochemie, Universität Leipzig, Brüderstrasse 34, 04103 Leipzig, Germany*

§*School of Chemistry, Food and Pharmacy, University of Reading, Whiteknights, Reading RG6 6AD, UK*

E-mail: andre.cobb@kcl.ac.uk

Abstract

In this study, we have developed a highly enantioselective organocatalytic route to the (1*S*,2*R*)-2-(aminomethyl)cyclopentane-1-carboxylic acid monomer precursor, which has a *cis*-configuration between the C- and N-termini around the cyclopentane core.

Kinetic measurements show that the product distribution changes over time due to epimerization of the C1 center. Computations suggest the *cis*-selectivity is a result of selective C-C bond formation, whilst subsequent steps appear to influence the selectivity at higher temperature. The resulting γ-amino acid residue was incorporated into a novel γ/α-peptide which forms a well-ordered 10/12-helix with alternate H-bond directionality in spite of the smallest value of the ζ-angle yet observed for a helix of this type. This highly defined structure is a result of the narrow range of potential ζ-angles in our monomer. In contrast, the larger range of potential ζ-values observed for the corresponding *trans*-system can be fulfilled by several competing helical structures.

Introduction

Foldamers – non-natural oligomers capable of forming secondary structures[1–6] - represent an intriguing class of macromolecules whose utilities range from molecular recognition[7,8] and peptidomimetics[3,4,9–11] to catalysis[12–15] and drug delivery.[16–18]

Chief amongst these systems are the peptidic foldamers which are comprised of non-natural amino acid monomers. There are two main reasons for the interest they have garnered. First is their potential to generate new and fascinating architectures, capable of displaying side chains in different ways compared to native structures. Second and important from a biological perspective, is that these systems are resistant to protease degradation – an important facet in peptidomimetics.[19]

One of the most successful approaches to ensuring that these non-natural units are capable of facilitating secondary structure formation is to design them such that they are conformationally restricted. This ensures that the relative arrangement of the C- and N-termini are fixed within the optimal parameters required for secondary structure formation.[20–22]

For these reasons, the asymmetric synthesis of conformationally restricted β- and γ-amino acids has received a great deal of attention, as has their application to foldamer design. The reason for desiring such diversity is simple – the more monomers one can access, the more

secondary structures become available and thus a greater range of exploitable chemical space is accessible, which is of great importance in fields such as peptidomimetics and catalysis. Several monomers of this type have been utilized to these ends,[23–26] but one that has been particularly elusive, owing to a lack of synthetic access to it has been the *cis*-cyclopentyl γ-amino acid system. In this report, we describe the organocatalytic development of this simple but challenging monomer, which uncovers an intriguing model of selectivity and we also demonstrate that it forms a highly organised and stable 10/12-helix beyond that observed for the corresponding *trans*-system.[25]

Results and discussion

cis-γ-Cyclopentane Amino Acid Synthesis.

We have ourselves contributed extensively to the asymmetric synthesis of conformationally restricted unnatural amino acids, including six-membered γ-amino acids or their precursors (*e.g.* **2**, Scheme 1a)[27] as well as other five-membered systems[28,29] and linear δ^3-amino acids.[30] At the same time, Gellman reported a synthesis of the related *cis*-cyclohexyl system **5** (Scheme 1b)[23] using secondary amine catalysis, and recently used the same approach to access the analogous *trans*-five-membered system **7** (Scheme 1c).[25] However, we desired access to a five-membered γ-amino acid with a *cis*-arrangement around the ring as we were curious about what the effect of this more conformationally restrained geometry would be when incorporated into a foldamer. Having successfully demonstrated that an organocatalytic 5-*exo*-*trig* can lead to *cis*-selectivity in a different process,[29] we felt that a similar intramolecular approach would be our best chance of attaining our desired *cis*-target with good selectivity. The only previous access to this system was achieved by Ley and co-workers who obtained the *cis*-γ-amino acid residue in 10% enantiomeric excess over 7 steps, using an enzyme-mediated resolution.[31]

We therefore decided to return to secondary amine catalysis in order to accomplish this,

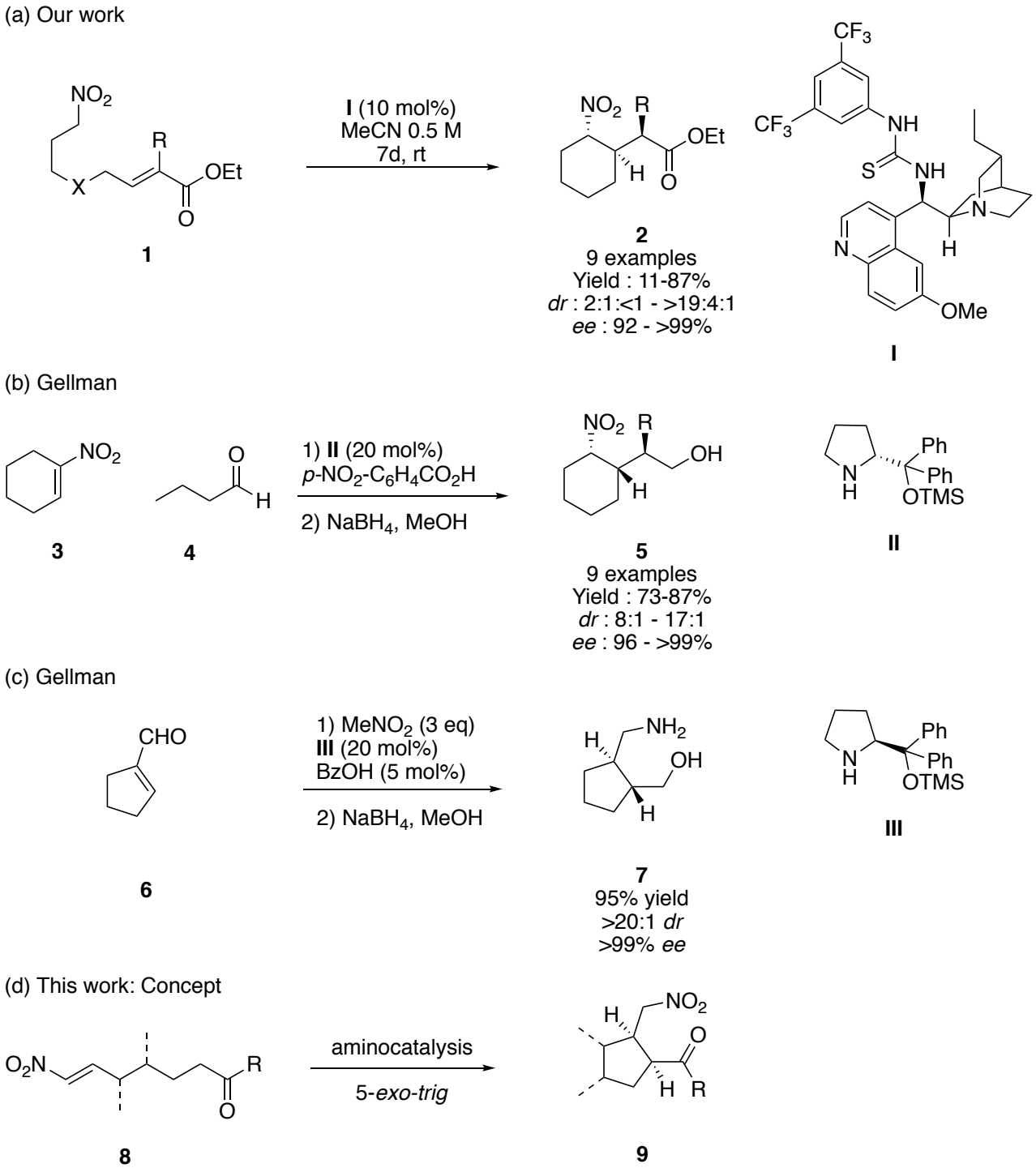

Scheme 1: (a) Our previous work on unnatural γ-amino acid synthesis.[27] (b) Gellman and co-workers' access to *trans*-cyclohexane γ-amino acid precursor.[26] (c) Gellman and co-workers' access to *trans*-cyclopentane γ-amino acid precursor.[25] (d) We theorized that we would be able to access the *cis*-system through a stereoselective intramolecular nitro-Michael addition.

with the view of using enamine chemistry to access the desired *cis*-cyclopentane system *via* an intramolecular conjugate addition onto a nitro-olefin (Scheme 1d). We began our efforts with the most basic 7-nitro-hept-6-en-1-al system **10**, made in 4 steps from cyclohexene (for full technical details, see SI), and were delighted to observe that the substrate was rapidly converted to the desired cyclic structure **11**, following an *in situ* reduction with sodium borohydride to prevent possible epimerization (Table 1).

In these initial screens, the preference for the *cis*-isomer did not appear to be strong at first. However, we were pleased to see that enantioselectivities were reasonable – particularly with respect to the Ley-Yamamoto-Armuddsen tetrazolic organocatalyst **VI** (Table 1, Entry 6).[32–38] It was noted with some interest at this stage that the enantioselectivities of the two isolated *cis*- and *trans*-products were markedly different and our rationale for this is discussed later in the manuscript. Nevertheless, in order to continue optimizing both diastereo- and enantioselectivity, we began by lowering the temperature to find to our delight that for the tetrazolic catalyst **VI** although the enantioselectivity was not affected, the diastereoselectivity was much improved (albeit at the expense of reaction time, Entry 8). Intriguingly, neither co-catalyst nor organocatalyst loading improved selectivities (see SI for full study) but a major influence was both the solvent (dichloroethane) and the *concentration* of the reaction, where although a more dilute system made the reaction much slower, both diastereoselectivity and enantioselectivity improved remarkably (Entry 14). Of particular note, with these optimized conditions, the reaction is scalable up to 7 mmol maintaining yields and selectivities.

Pleasingly we were able to deduce the absolute stereochemistry of our product from the single-crystal X-ray diffraction of the corresponding (-)-camphonyl ester **12** which confirmed a (1*S*,2*R*)-configuration. (Figure 1).

Although we had now managed to access our desired target for foldamer design in excellent stereoselectivity, we also wished to see if our methodology could be applied to other substrates. In that respect, we were able to access cyclopentylketone **13** from the corre-

Table 1: Optimisation Study (Abridged)[a]

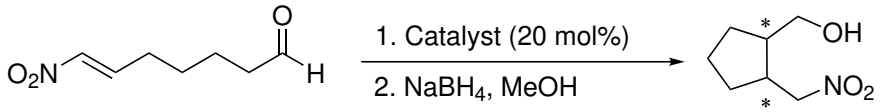

10 **11**

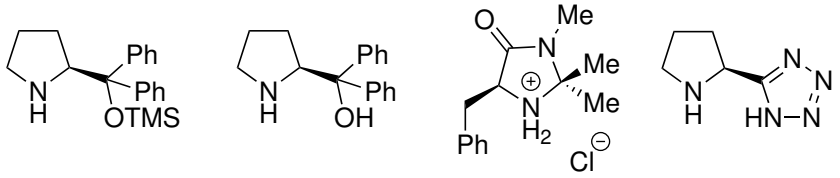

III **IV** **V** **VI**

Entry	Catalyst	Solvent	Conc, M	T, °C	Time, h[b]	Yield, %[c]	*dr*,[d] *cis:trans*	*ee*,[e] %
1[f]	**III**	CH_2Cl_2	0.2	rt	0.3	62	1:4	nd,-59
2[f]	**VI**	CH_2Cl_2	0.2	rt	1.5	91	1:8	nd, 72
3	**III**	CH_2Cl_2	0.2	0	1	57	1:1	-87,[g]-27
4	**IV**	CH_2Cl_2	0.2	0	96	5[h]	1:1	nd,nd
5	**V**	CH_2Cl_2	0.2	0	72	42	1:6	-68,-74
6	**VI**	CH_2Cl_2	0.2	0	14	62	2:1	83,[g] 71
7	**III**	CH_2Cl_2	0.2	-20	>24	20	1:1	36, 53
8	**VI**	CH_2Cl_2	0.2	-20	22	62	3:1	82, 22
9	**VI**	MeCN	0.2	-20	25	54	1:1	65, 56
10	**VI**	THF	0.2	-20	24	52	1:1	50, 38
11	**VI**	MeOH	0.2	-20	26	11	3:2	-10
12	**VI**	DCE	0.2	-20	50	53	7:1	85, 54
13	**VI**	DCE	0.1	-20	48	66	6:1	89
14	**VI**	DCE	0.05	-20	168	74	17:2	93
15	**VI**[i]	DCE	0.05	-20	168	43	10:1	92,-11

[a] See Supporting Information for full optimization study. [b] Time for complete consumption of aldehyde as observed by tlc. [c] Isolated yield over two steps. [d] Determined by ^{1}H NMR on the crude mixture. [e] Determined by HPLC analysis using a chiral OD column for the *cis* diastereomer and a chiral AS column for the *trans* diastereomer. [f] Yield, *dr* and *ee* were calculated of the aldehyde product without any further reduction with $NaBH_4$. [g] Determined by HPLC analysis using a chiral AD-H column. [h] Reaction did not go to completion. [i] 2 mol% of catalyst loading.

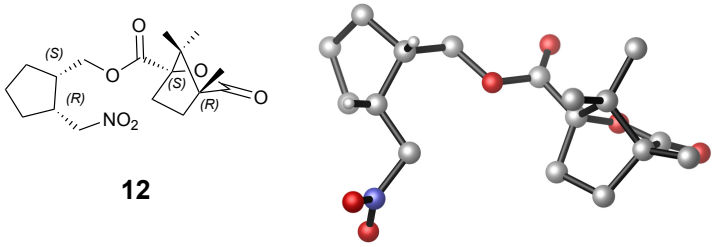

12

Figure 1: X-ray crystal structure of the alcohol derivative (CCDC : 1947228) **12**.

sponding nitroolefin substrate, as well as the fascinating indane system **14** albeit with a 1:1 diastereomeric ratio. Nevertheless, the excellent enantioselectivities of the isolated *cis*-systems was very pleasing (Figure 2).

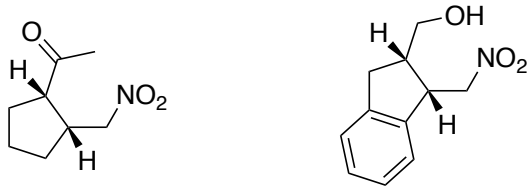

13
56%
dr 1:1
cis 84% *ee*

14
73%
dr 1:1
cis 90% *ee*

Figure 2: Our methodology could be applied to simple ketones as well as the intriguing indane system **14**.

As briefly mentioned above, during our studies it became apparent that the diastereoselectivity and enantioselectivity of this reaction was not straightforward. To begin with, the enantioselectivity of the *cis*-conformer was far superior to that of the *trans*-conformer. Additionally, it was observed that prolonged reaction times would not only decrease the diastereomeric ratio of the *cis*- and *trans*-adducts, but also that the enantiomeric excesses of these were changeable, with the *cis*-system being degraded and the *trans*-one being enhanced. We theorized two possibilities for this time dependent selectivity. First, that the simple reverse reaction could be occurring, ultimately resulting in the thermodynamically favourable *trans*-system becoming more predominant *via* a less enantioselective transition state. Second that there are two independent and competing pathways to the *cis*-and *trans*-

adducts that over time are subjected to a catalyst-assisted epimerization through a product enamine. Examining the ratio of the four enantiomers during and after the reaction, one can notice a redistribution driven by thermodynamics converting both *cis*-products to their respective C1-epimeric *trans*-products (Figure 3).

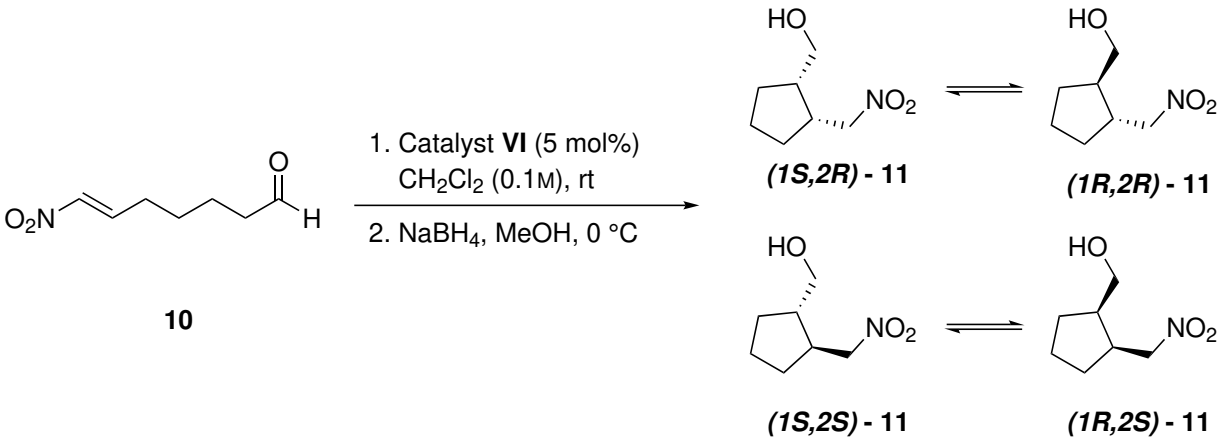

(a)

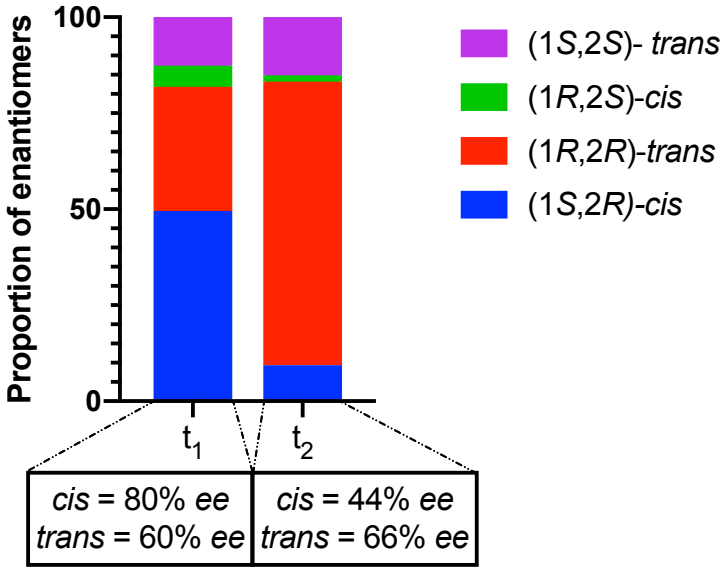

(b)

Figure 3: Proportion of enantiomers of the five-membered ring **11** at t_1 and at t_2 performing the reaction in CH_2Cl_2 at rt for investigative purposes.

Figure 3b shows the ratio of each enantiomer at t_1 (2 hours from beginning of reaction) and at t_2 (23 hours from beginning of reaction). Interestingly, the decrease of concentration of the (1*S*,2*R*)-*cis*-enantiomer matches with the increase in concentration of the (1*R*,2*R*)-*trans*-

enantiomer, and similarly, the ratio difference of the (1*R*,2*S*)-*cis* enantiomer matches with the ratio difference of the (1*S*,2*S*)-*trans* enantiomer. This suggests that the major (1*S*,2*R*)-*cis*-enantiomer is converted to the (1*R*,2*R*)-*trans*-enantiomer and the minor (1*R*,2*S*)-*cis*-enantiomer is converted to the (1*S*,2*S*)-*trans*-enantiomer, implying that C1-epimerization is certainly one aspect of the story.

Theoretically, a retro-Michael reaction could also lead to the conversion of *cis*-enantiomers to the thermodynamically more favoured *trans*-enantiomers. Interestingly, however, this study shows that the enantiomeric ratio of the *trans*-product is not maintained as one would expect if this were the case, but instead undergoes an enantioenrichment.

Computational Investigation of Stereoselectivity.

In order to gain a complete understanding of this, we turned to computational studies to ascertain the most energetically likely pathways in the formation of each diastereomer. Calculations were performed for substrate **10** in the presence of catalyst **VI**. Our goal was to establish a model which accounts for the initial *cis*-selectivity and its observed change in enantiomeric excess over time. Conformational sampling was carried out using mixed low-mode Monte-Carlo search[39–41] as implemented in Schrodinger 2017-1[42] based on the OPLS 2005 all atom force field,[43–45] followed by conformational clustering. Kohn-Sham DFT calculations were done for the mechanistic studies using Gaussian09 Rev.E.[46] The presented result were obtained employing the ωB97XD range separated hybrid functional,[47] with the basis 6-311G(d,p) for optimization, frequency and solvent calculations and the 6-311++G(3df,3pd) basis for electronic energies.[48–50] Thermochemical corrections were calculated according to Grimme's qRRHO[51] approximation as implemented in goodvibes.[52] Solvent corrections are determined for DCE using PCM solvent model with Truhlar's SMD parametrization.[53,54] The proposed catalytic cycle is depicted in Scheme 2.

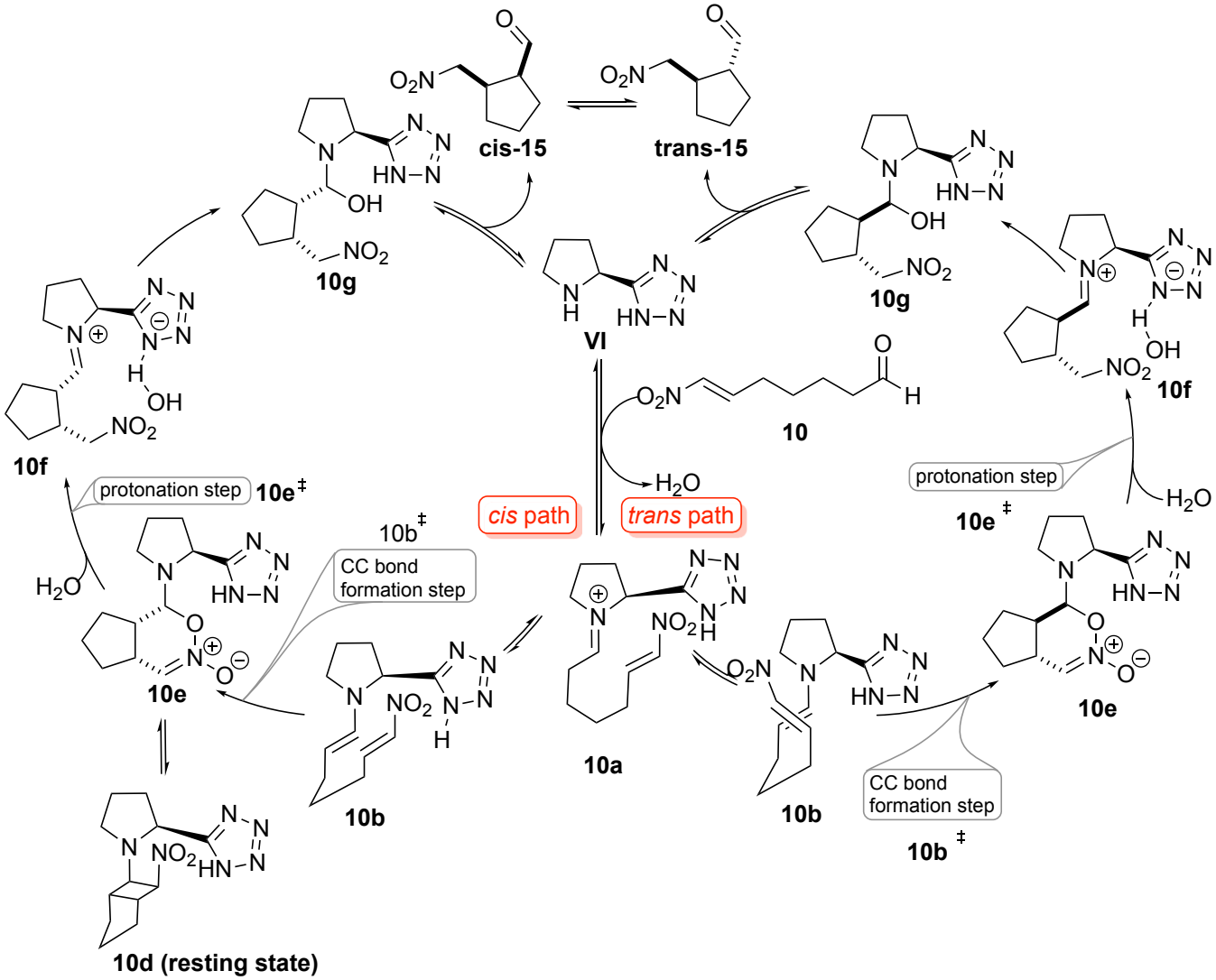

Scheme 2: Mechanistic proposal of the 5-*exo-trig* cyclisation.

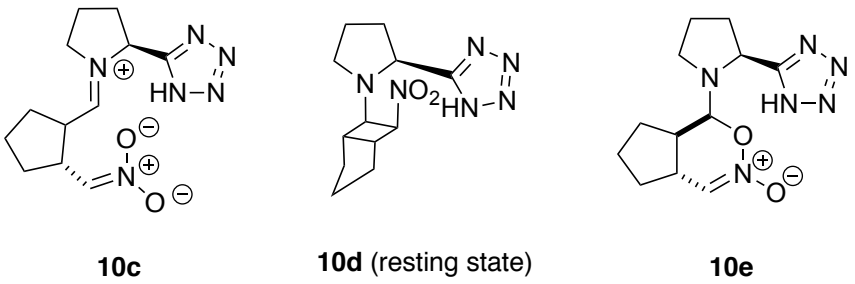

Figure 4: Possible intermediates after the CC bond formation.

We focused on the carbon-carbon bond forming and the subsequent protonation step as well as the intermediates connecting them as they have been shown to be of paramount

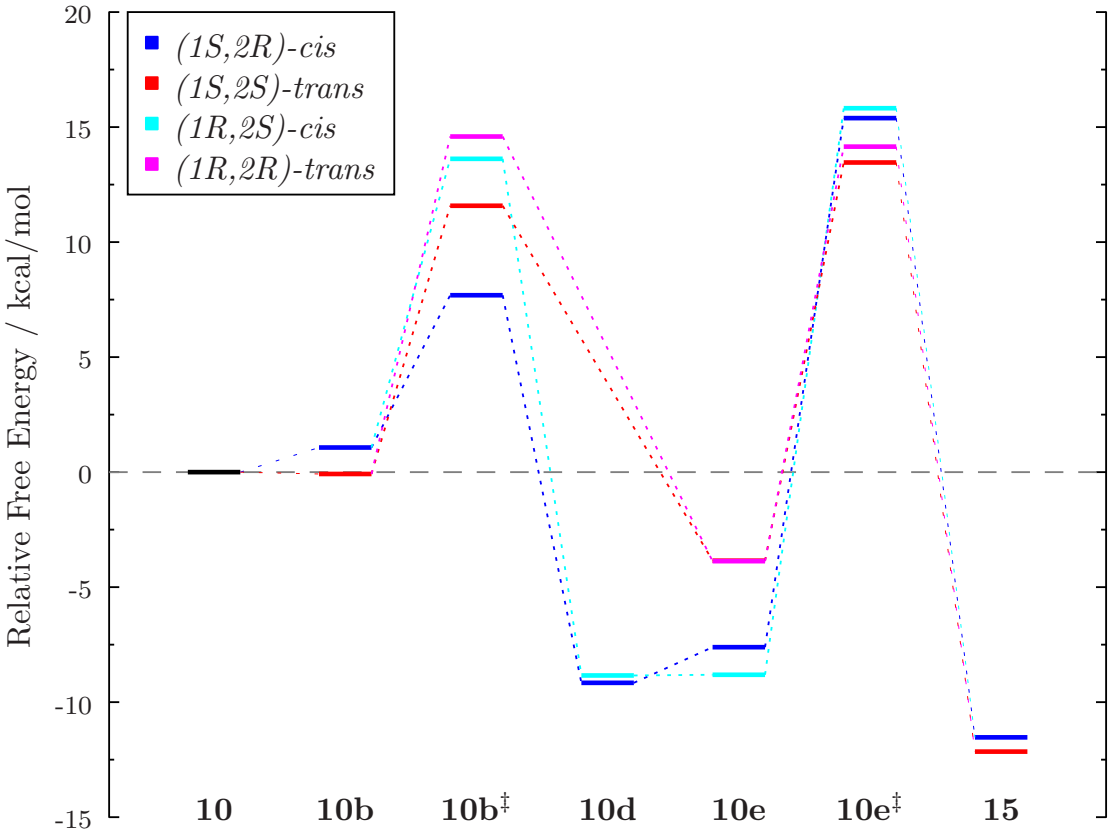

Figure 5: Calculated energies and Gibbs free energies were obtained at the ωB97XD/6-311G(d,p) level of theory with qRRHO corrections and SMD solvation in dichloroethane.

importance. The transition states of the addition step shed light on the coordinating nature of the tetrazole moiety of the catalyst. The most stable conformers feature a strong H-bonding interaction between the tetrazole ring which is maximized in the path of the product (1*S*,2*R*)-**15** (Figure 6), with a small cost of strain in the pyrrolidine ring.

In a similar manner to the intermediates observed by Seebach and Hayashi,[55] Blackmond,[56–59] Wennemers,[60] Pihko and Papái[61,62] in studies performed with the Hayashi-Jørgensen catalyst, there are three intermediates the addition step can result in (Figure 4). In a moderately polar solvent as DCE, the zwitterionic structure **10c** is thermodynamically unfavoured. The formation of a four-membered ring (**10d**) in a *trans*-configuration is rendered impossible due to extreme ring strain, while it is found to be rather stable in the *cis*-path, (even if the applied level of theory might overestimate its stability). Thus the

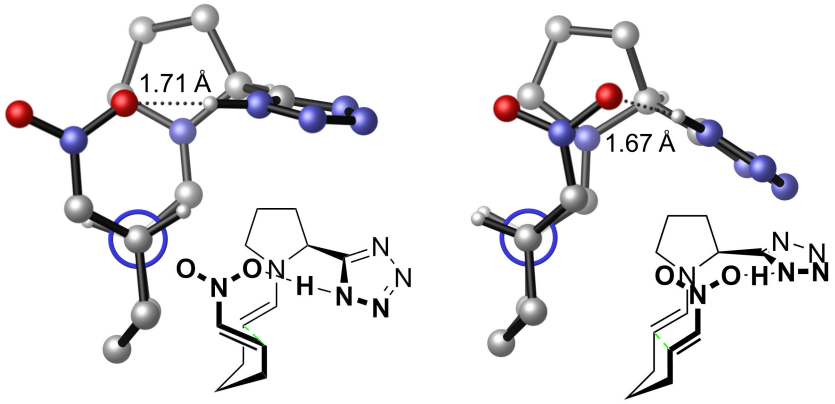

Figure 6: C-C bond forming transition states on the (1*S*,2*S*) (left) and (1*S*,2*R*) (right) paths.

oxazine oxide (OO) **10e** intermediate is left the sole option in the *trans*-path, as shown in Scheme 2. In the absence of co-catalyst, the addition of the previously condensed water to form the product hemiaminal can happen in two ways. Either the oxygen undergoes a nucleophilic attack on the iminium carbon, which is unlikely, since in abundant intermediates the centre does not bear a positive charge, or the water protonates the nitronate moiety, ultimately breaking the auxiliary ring formed in the intermediates. The superiority of the latter scenario is further underlined by the assistance of the tetrazole ring once again, acting as a Brønsted acid to stabilize the transiently forming hydroxide anion. This structure quickly results in formation of the product hemiaminal (**10g** in Scheme 2). Interestingly, the protonation step favours the *trans* products, because the ring configuration enables a more concerted set of bonds forming and breaking as depicted in 7. The overall free energy profile is shown in Figure 5. The relative free energies of the transition states of the aforementioned steps are close to each other. Due to the involvement of the water in the second step, the thermodynamic corrections, introduced as Grimme's qRRHO,[51] increase the uncertainty of the comparison of these steps, possible overestimating the barrier of the protonation step. Nevertheless, the temperature dependence of the qRRHO term of the protonation transition state is considerably higher than that of the first step, which may also account for the temperature dependent selectivity (see SI for full details).

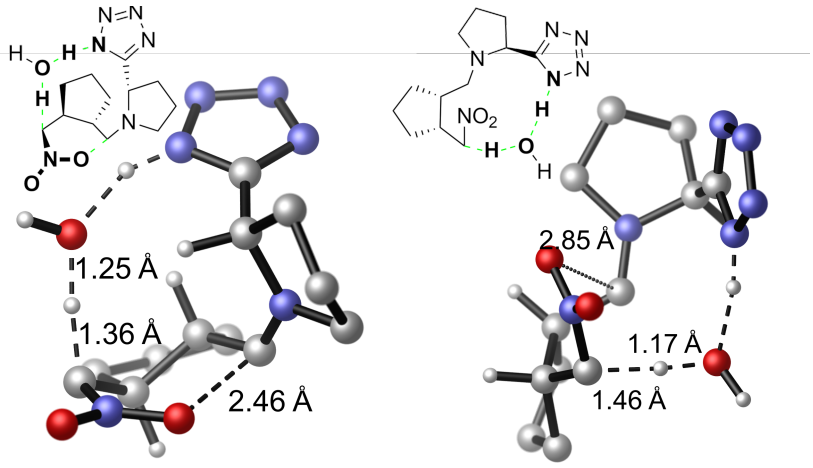

Figure 7: **left**: geometry of (*1S,2S*)-**1e**‡. **right**: geometry of (*1S,2R*)-**1e**‡, showing an earlier, less concerted TS.

Assuming that the addition step determines the selectivity, *cis* diastereomers form faster and with higher enantioselectivity. This model is in line with the experimental evidence shown in Figure 3 for the C1 epimerization where (1*S*,2*R*)-**15** and (1*R*,2*S*)-**15** convert to (1*R*,2*R*)-**15** and (1*S*,2*S*)-**15**, respectively.

In summary, the existence of two independent pathways to the *cis*- and *trans*-adducts has some unexpected consequences. First, for reasons explained in the selectivity model, the *ee* of the *cis*- is superior to that of the *trans*-adduct. Second, that this *cis*-product can epimerise to the *trans*-adduct under the reaction conditions.

If the *trans*-product was solely formed by epimerization of the *cis*-adduct, the enantiomeric excess would be the same. However, although this C2-epimerization is clearly happening (with the products of this being of the same high enantiopurity), it is also being incorporated into the original *trans*-selective pathway which is, as mentioned, of a much lower enantioselectivity. As a consequence the overall impression given is that the *trans*-adduct becomes increasingly enantioenriched as more of the corresponding and purer *cis*-adduct epimerises to it. On the other hand, the enantioselectivity of the *cis*-enantiomer decreases with time and this can be simply explained by the fact that the high difference of concentration of the two enantiomers leads to the epimerization in greater quantities of the major

cis enantiomer, likely *via* 1^{st} order kinetics, and ultimately adversely effecting the *er* of that system.

Structural Characterisation of γ/α-Foldamers Containing the *cis*-Cyclopentyl Monomer.

Following both ours,[27] and the Gellman group's[23–26] syntheses of γ-amino acids, their use within foldamer constructs has attracted great interest. In the main these systems have employed a cyclic backbone; a common feature which results in a conformational restriction that is beneficial for foldamer formation. For example, Gellman has accessed foldamers based on *cis*- and *trans*-cyclohexyl based γ-systems (**A**, **B** and **C** in Figure 8).[23,24,26] Of particular note is also the Balaram and co-workers' α/γ-peptide containing the constrained achiral γ-residue gabapentin (**D**, Figure 8).[63,64] System **D** allowed the arrangement of the secondary structure which contained, until now, one of the smallest ζ-angles known and leading to a 12/10-helix. The *trans*-cyclopentyl system has also been exploited (**E**, Figure 8) but a noticeable absence from these studies have been the *cis*-cyclopentane γ-amino acids that are the subject of this study (Figure 8) owing to the aforementioned lack of methodology towards them in any enantiopure sense.

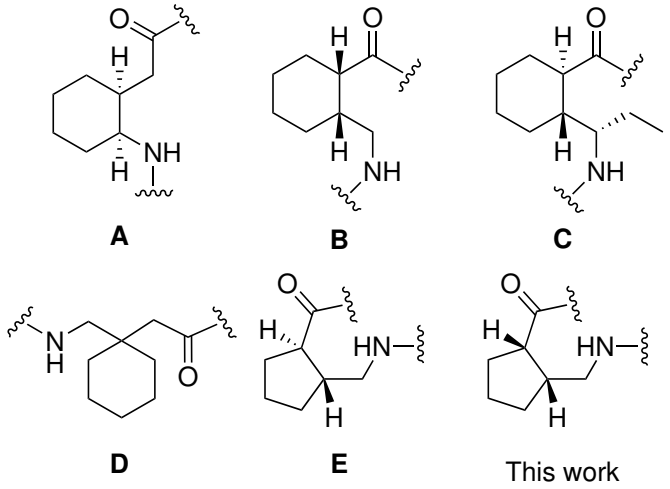

Figure 8: Constrained carbocyclic γ-amino acids that promote helical foldamers.

Having successfully achieved the synthesis of the *cis*-γ-amino acid precursor **11**, our next task was to synthesize the corresponding 1:1 γ/α-hexapeptide for secondary structure analysis and this is summarized in Scheme 3.

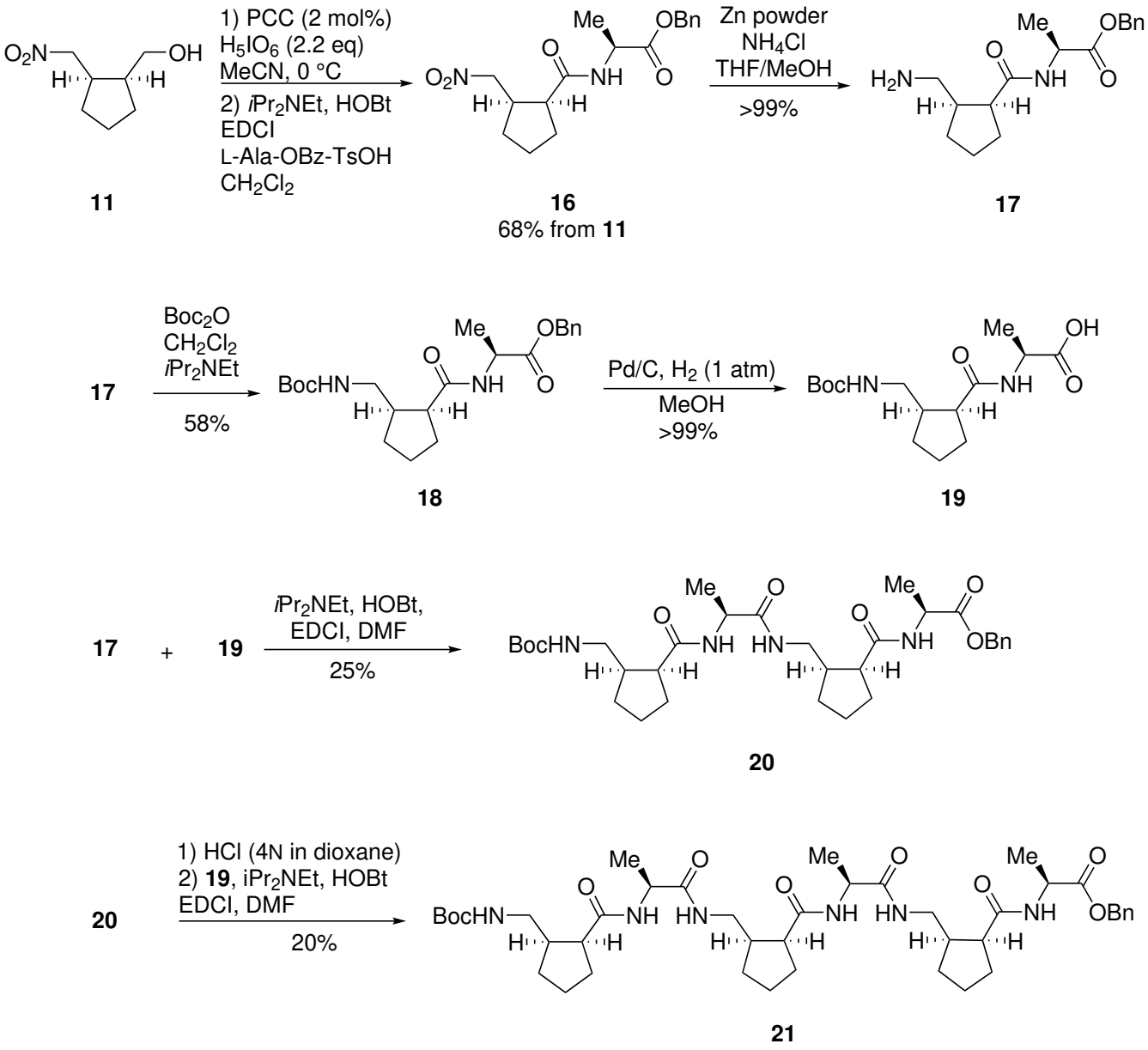

Scheme 3: γ/α-Peptides **18**, **20** and **21** synthesis.

To begin with, dipeptide precursor **16** was accessed through the PCC oxidation of γ-nitroalcohol **11** followed by peptide coupling with benzoyl protected L-alanine. The resulting species was then reduced using zinc powder to unmask the primary amine which was protected using Boc anyhydride, giving C-terminus protected NH_2-dipeptide-OBn **17**. Boc protection of dipeptide **17** then allowed us to access to the N-terminus protected BocNH-dipeptide-OH derivative **19** using standard reduction conditions. The crystalline nature of intermediate **18** enabled collection of single-crystal X-ray diffraction data, which not only confirmed the configuration of our cyclopentane system, but also allowed us to analyse the internal torsional angles of our γ-residue (Figure 9).

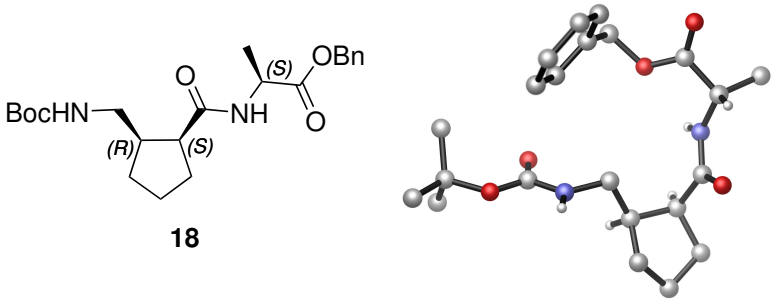

Figure 9: Asymmetric unit of the single-crystal X-ray structure of Boc-protected dipeptide **18** (CCDC : 1947227).

With dipeptides **17** and **19** in hand, we were able to couple them to generate tetramer **20**. The N-terminus of this was then exposed on treatment with HCl in dioxane, allowing for the coupling of a second dipeptide **19** and finally access to the desired hexapeptide system **21** (Scheme 3). Owing to the short length of tetramer **20**, we focused on the structural characterisation of the hexamer **21**.

The very good dispersion of proton signals allowed for the near total assignment based on ^{1}H-^{1}H COSY, ROESY and TOCSY NMR. Four out of six amide peaks were found at $\delta >$ 7 ppm, which is a typical feature of H-bonded protons (Figure 10). A self-aggregation experiment was performed to prove there was no self-association and confirm that the downfield detected amide peaks were due to intramolecular rather than intermolecular interactions (0.04 - 4mM in $CDCl_3$, see full details in the SI).

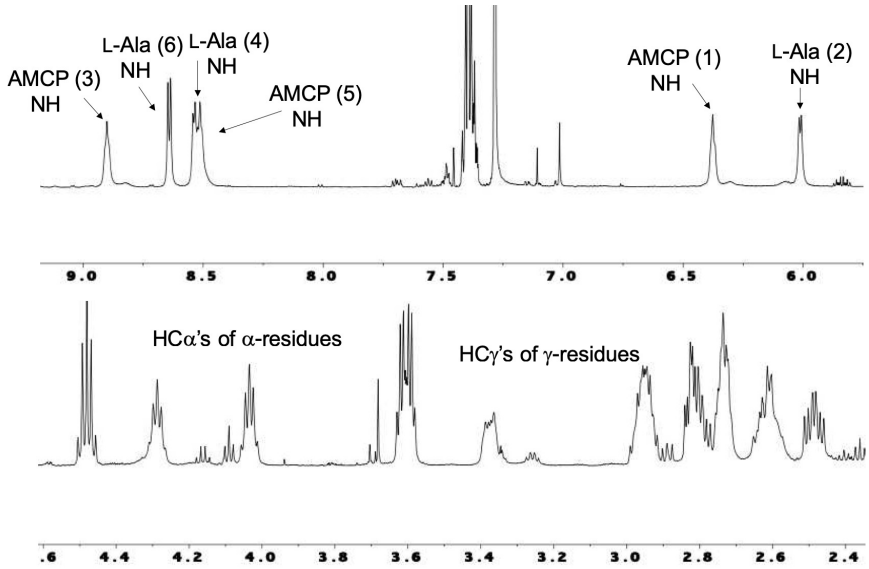

Figure 10: ^{1}H NMR spectra in $CDCl_3$ at a concentration of 0.2 mM for the characterisation of γ/α peptide **21**.

DMSO titration experiments were then conducted to identify protons that were not engaged in intramolecular H-bonding, thus discriminating free and H-bonded signals giving further structural information. Figure 11b shows the change in chemical shift ($\Delta\ \delta$) of each residue after consecutive additions of DMSO (5, 10, 15, 25, 50, 100 µL). Only the L-Ala (2) amide peak, which is highlighted in red, is strongly shifted downfield after the addition of DMSO and thus is the only residue not involved in H-bonding (Figure 11), giving further support to the proposed helical structure.

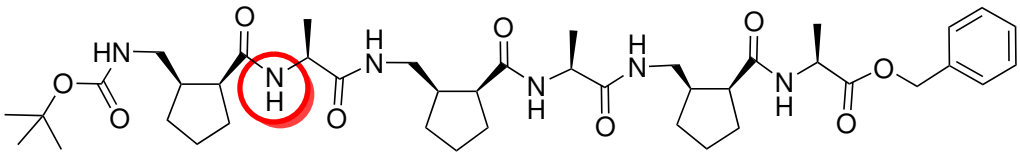

(a)

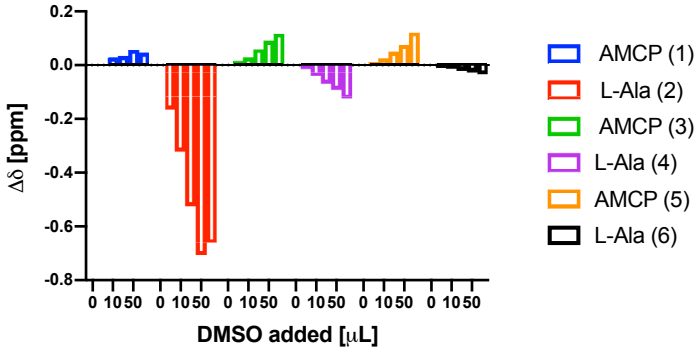

(b)

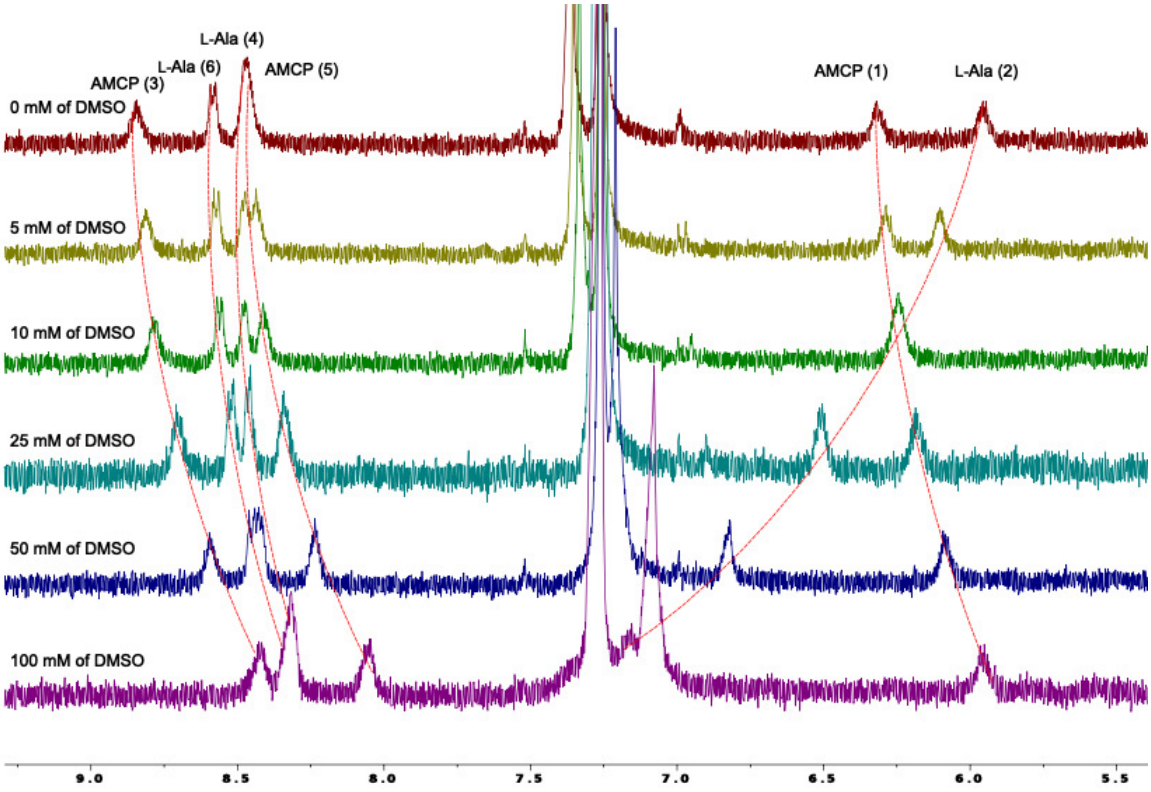

(c)

Figure 11: DMSO titration of 2mM γ/α-peptide **21** in $CDCl_3$: (a) H-bonding and solvent exposed amide protons in the proposed γ/α-peptide 10/12-helical structure. The amide proton circled in red are expected to exhibit the largest chemical shift change upon DMSO addition. (b) Change of chemical shift of NH peaks with progressive DMSO addition. (c) Amide peak region of ^{1}H NMR spectra collected with addition of 0, 10, 25, 50 and 100 µL of DMSO added to a 2mM solution of hexamer **21** in $CDCl_3$.

This was further supported by detailed analysis of the obtained 2-D NMR data, which showed three medium range cross peaks (Types i, ii and iv in Table 2), characteristic of 12/10-helices for α/γ-peptides[25,26,65] (relative positions of interacting amino acids $\gamma_1 \rightarrow \alpha_2/\gamma_1 \leftarrow \alpha_4$) and therefore of a 10/12-helical structure for γ/α-peptides($\alpha_1 \rightarrow \gamma_2/\alpha_1 \leftarrow \gamma_4$, 2).[21] Like Gellman we do not see interaction iii,[25] however we do see interaction iv, which might be one reason that we see a more ordered structure.[26,65] In addition, the different sequencing might have led to additional NOE interactions, and therefore we also observed strong interactions between HCα of α residues with HCβ of *i +1* α-residues and HCγ of γ-residues with HCα of the i+2 γ-residues (Table 2).

The determined NOE cross peaks were used as molecular restrictions to identify the most populated lowest energy conformations of the γ/α-peptide **21**. Based on the NMR data, 55 conformers of the hexapeptide were identified employing Monte-Carlo methods (details in SI) and further optimized with DFT empoying the long range corrected ωB97XD functional together with the 6-311G** basis set.[47] The overlay of the conformers above 1% population (assuming Boltzmann distribution) is depicted in Figure 12. Five out of six residues correspond clearly to a well defined 10/12-helix with backbone dihedral values listed in Table 3.

Most interesting is examination of the backbone torsion angle ζ, representing rotation around the bond of the cyclopentane ring that is part of the peptide sequence. The values for this angle are strongly restricted in case of the *cis*-configuration on this bond. In the case of (*1S,2R*)- or, alternatively, (*1R,2S*)-configuration, theoretical studies show that only a relatively small range of values of about 0°, ±30° or ±45° are possible, dependent on which bond of the envelope conformation of the ring is selected to be part of the peptide sequence (pseudorotation). In good agreement, the values for ζ from the NMR analysis are in between 30-45°. Based on quantum chemical calculations, a catalog of all helical folding patterns in conformationally unrestricted α/γ-peptides is available.[21] Comparing our structure with the catalogue data shows that it corresponds to the most stable mixed 12/10-helix in the

Table 2: Significant observed NOE cross peaks for hexamer **21** and characteristic NOE cross peaks of 12/10-helical structures.

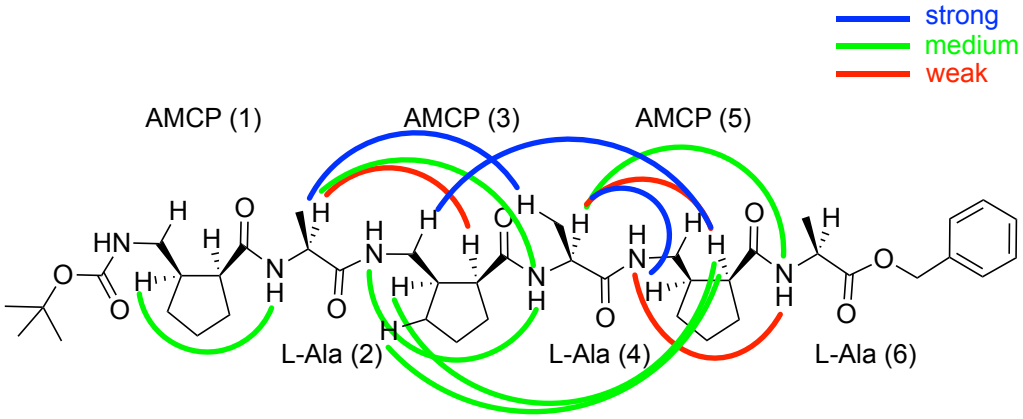

(i) HC[α] of [α]-residue (i) to NH of [α]-residue (i + 2) **strong and medium**
(ii) NH of [γ]-residue (i) to NH of [α]-residue (i+ 1) **medium and weak**
(iii) HC[γ] of [γ]-residue (i) to NH of [α]-residue (i +1) **not observed**
(iv) HC[α] of [α] residue (i) to HC[α] of [γ]-residue (i +1) **weak**
(v) NH of [γ]-residue (i) to HC[α] of [α]-residue (i +1)

NOE cross peak	NMR distance Å	Designation
HCα (2) - HCα (3) - iv	**4.28**	**weak**
HCα (2) - NH (4) - i	**3.47**	**medium**
HCα (2) - HCβ (4)	2.99	strong
NH (3) - NH (4) - ii	**3.46**	**medium**
HCγ''(3) - HCα (5)	2.62	strong
HCα (4) - HCβ (5)	2.96	strong
HCα (4) - NH (6) - i	**3.47**	**medium**
HCα (4) - HCα (5) - iv	**3.96**	**weak**
NH (5) - NH (6) - ii	**3.79**	**weak**

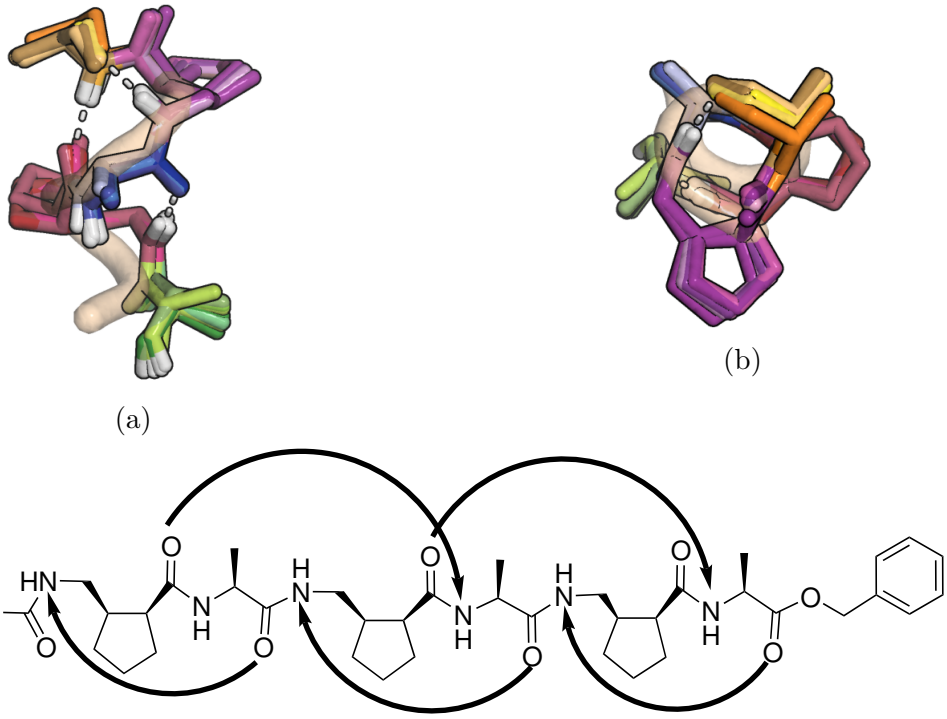

Figure 12: Overlap of the 9 lowest energy structures of **21** obtained with a computational study where residue AMCP (1) and side chains have been omitted, as well as simplification of the terminal protecting groups for the purposes of clarity. (a) Backbone of oligomer **21**. (b) Top view of helical backbone structure of **21**. (c) H-bond directionality for the oligomer **21**.

Table 3: Backbone torsion angles of hexamer **21** from NMR analysis[a] and X-ray data for dipeptide **18**.

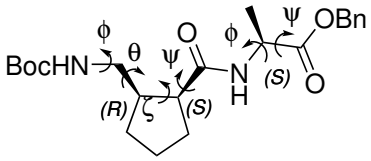

18

	Residue	ϕ	θ	ζ	ψ
Hexamer **21**	AMCP (1)	26.0±75	9.7±50	35.3±23	-103.0±8
	L-Ala (2)	-72.8±8	-	-	128.7±34
	AMCP (3)	61.0±3	43.5±3	41.9±1	-119.0±4
	L-Ala (4)	-72.8±4	-	-	141.7±2
	AMCP (5)	59.0±1	46.2±2	28.4±1	-119.7±3
	L-Ala (6)	-63.9±1	-	-	139.9±10
X-ray Dipeptide crystal **18**	*cis*-AMCP (1)	-96.3	176.7	29.4	-100.1
	L-Ala(2)	-125.7	-	-	1.1

[a] ωB97XD/6-311G** level of density functional theory.

catalogue. The backbone torsion angles of the idealized helix are $\phi = 66°$, $\theta = 32°$, $\zeta = 48°$, ψ = -129° for the γ-amino acid constituent and ϕ = -67° and $\psi = 148°$ for the α-amino acid constituent. The same helix type was also found by Balaram and co-workers in α/γ-peptides with the γ-amino acid gabapentine.[63]

The situation is distinctly different in case of a *trans*-arrangement on the cyclopentane ring with *1S,2S*- or *1R,2R*-configuration. Here, a much larger range of possible values for the torsion angle ζ are possible, which occur in a greater number of potential helical structures. Thus, competition between these *trans*-structures may prevent stable secondary structure formation. Indeed, studies on peptides with such constituents by Gellman and coworkers[25] indicate a much weaker tendency to form ordered helical structures, although a tendency in direction of a 10/12-helix found by Sharma and coworkers[65] became visible.

Conclusions

In conlusion, we have developed a highly stereoselective organocatalytic route to the (1*S*,2*R*)-2-(aminomethyl)cyclopentane-1-carboxylic acid monomer precursor. This selectivity has

been explained computationally and found to be a result of two independent pathways with a favourable kinetic profile towards the *cis*-system. Prolonged reaction times erode both the enantiopurity of the *cis*-adduct and the diastereomeric ratio *via* C2-epimerization that unusually also leads to the apparent enantioenrichment of the *trans*-adduct. γ/α-Oligomers were then synthesized and it was found that the hexamer populated a 10/12-helix. The *cis*-γ-residue contains the smallest ζ-angles reported for this type of helix and in contrast to the one reported by Balaram and co-workers[63] the helix seems tighter due to the even smaller ζ-angles. This highly organized secondary structure does not seem to occur in the corresponding *trans*-system, possibly owing to the greater number of potential conformations in that system resulting in a greater range of helices.[25]

Acknowledgement

We would like to thank our funders King's College London (to. R. F.) and the ERC (Project No. 757850 BioNet to D. B. and T. F.). We are grateful to the UK Materials and Molecular Modelling Hub for computational resources, which is partially funded by EPSRC (EP/P020194/1). D.B. and E.R. are grateful for the Nuffield Foundation and the summer students Angelo Davis and Fangling Zheng for their commitment.

Supporting Information Available

Experimental procedures and characterization data for all new compounds.

References

(1) Martinek, T. A.; Fülöp, F. Peptidic foldamers: Ramping up diversity. *Chemical Society Reviews* **2012**, *41*, 687–702.

(2) Guichard, G.; Huc, I. Synthetic foldamers. *Chem. Commun* **2011**, *47*, 5933–5941.

(3) Hill, D. J.; Mio, M. J.; Prince, R. B.; Hughes, T. S.; Moore, J. S. A field guide to foldamers. *Chemical Reviews* **2001**, *101*, 3893–4011.

(4) Gellman, S. H. Foldamers: A manifesto. *Accounts of Chemical Research* **1998**, *31*, 173–180.

(5) Hecht, S.; Huc, I.; Huc, S. H.; Ivan, *Foldamers*; WILEY-VCH, 2007; pp 229–265.

(6) Yashima, E.; Maeda, K.; Lida, H.; Furusho, Y.; Nagai, K. Helical polymers: Synthesis, structures, and functions. *Chemical Reviews* **2009**, *109*, 6102–6211.

(7) Chandramouli, N.; Ferrand, Y.; Lautrette, G.; Kauffmann, B.; Mackereth, C. D.; Laguerre, M.; Dubreuil, D.; Huc, I. Iterative design of a helically folded aromatic

oligoamide sequence for the selective encapsulation of fructose. *Nature Chemistry* **2015**, *7*, 334–341.

(8) Collie, G. W.; Bailly, R.; Pulka-Ziach, K.; Lombardo, C. M.; Mauran, L.; Taib-Maamar, N.; Dessolin, J.; Mackereth, C. D.; Guichard, G. Molecular Recognition within the Cavity of a Foldamer Helix Bundle: Encapsulation of Primary Alcohols in Aqueous Conditions. *Journal of the American Chemical Society* **2017**, *139*, 6128–6137.

(9) Cheng, R. P.; Gellman, S. H.; Degrado, W. F. β-peptides: From structure to function. *Chemical Reviews* **2001**, *101*, 3219–3232.

(10) Goodman, C. M.; Choi, S.; Shandler, S.; Degrado, W. F. Foldamers as versatile frameworks for the design and evolution of function. *Nature Chemical Biology* **2007**, *3*.

(11) Gopalakrishnan, R.; Frolov, A. I.; Knerr, L.; Drury, W. J.; Valeur, E. Therapeutic potential of foldamers: From chemical biology tools to drug candidates? *Journal of Medicinal Chemistry* **2016**, *59*, 9599–9621.

(12) Müller, M. M.; Windsor, M. A.; Pomerantz, W. C.; Gellman, S. H.; Hilvert, D. A rationally designed aldolase foldamer. *Angewandte Chemie - International Edition* **2009**, *48*, 922–925.

(13) Maayan, G.; Ward, M. D.; Kirshenbaum, K. Folded biomimetic oligomers for enantioselective catalysis. *Proceedings of the National Academy of Sciences of the United States of America* **2009**, *106*, 13679–13684.

(14) Nagano, M.; Doi, M.; Kurihara, M.; Suemune, H.; Tanaka, M. Stabilized α-Helix-Catalyzed Enantioselective Epoxidation of α,β-Unsaturated Ketones. *Organic Letters* **2010**, *12*, 3564–3566.

(15) LeBailly, B. A.; Byrne, L.; Clayden, J. Refoldable foldamers: Global conformational

switching by deletion or insertion of a single hydrogen bond. *Angewandte Chemie - International Edition* **2016**, *128*, 2172–2176.

(16) Douat, C.; Aisenbrey, C.; Antunes, S.; Decossas, M.; Lambert, O.; Bechinger, B.; Kichler, A.; Guichard, G. A Cell-Penetrating Foldamer with a Bioreducible Linkage for Intracellular Delivery of DNA. *Angewandte Chemie - International Edition* **2015**, *54*, 11133–11137.

(17) Douat, C.; Bornerie, M.; Antunes, S.; Guichard, G.; Kichler, A. Hybrid Cell-Penetrating Foldamer with Superior Intracellular Delivery Properties and Serum Stability. *Bioconjugate Chemistry* **2019**, *30*, 1133–1139.

(18) Aguesseau-Kondrotas, J. et al. Prospect of Thiazole-based g-Peptide Foldamers in Enamine Catalysis: Exploration of the Nitro-Michael Addition. *Chemistry - A European Journal* **2019**, *25*, 7396–7401.

(19) Giannis, A.; Kolter, T. Peptidomimetics for Receptor Ligands-Discovery, Development, and Medical Perspectives. *Angewandte Chemie-International Edition in English* **1993**, *32*, 1244–1267.

(20) Baldauf, C.; Günther, R.; Hofmann, H.-J. Helix Formation and Folding inγ-Peptides and Their Vinylogues. *Helvetica Chimica Acta* **2003**, *86*, 2573–2588.

(21) Baldauf, C.; Günther, R.; Hofmann, H.-J. Helix Formation in α,γ- and β,γ-Hybrid Peptides: Theoretical Insights into Mimicry of α- and β-Peptides. *Journal of Organic Chemistry* **2006**, *71*, 1200–1208.

(22) Baldauf, C.; Hofmann, H.-J. Ab initio MO Theory - An Important Tool in Foldamer Research: Prediction of Helices in Oligomers of ω-Amino Acids. *Helvetica Chimica Acta* **2012**, *95*, 2348–2383.

(23) Guo, L.; Chi, Y.; Almeida, A. M.; Guzei, I. A.; Parker, B. K.; Gellman, S. H. Stereospecific Synthesis of Conformationally Constrained γ-Amino Acids: New Foldamer Building Blocks That Support Helical Secondary Structure. *Journal of American Chemical Society* **2009**, *131*, 16018–16020.

(24) Guo, L.; Zhang, W.; Guzei, I. A.; Spencer, L. C.; Gellman, S. H. New Preorganized γ-Amino Acids as Foldamer Building Blocks. *Chem. Biodiversity* **2012**, *14*, 2582–2585.

(25) Giuliano, M. W.; Maynard, S. J.; Almeida, A. M.; Reidenbach, A. G.; Guo, L.; Ulrich, E. C.; Guzei, I. a.; Gellman, S. H. Evaluation of a cyclopentane-based γ-amino acid for the ability to promote α/γ-peptide secondary structure. *Journal of Organic Chemistry* **2013**, *78*, 12351–12361.

(26) Giuliano, M. W.; Maynard, S. J.; Almeida, A. M.; Guo, L.; Guzei, I. A.; Spencer, L. C.; Gellman, S. H.; S, S. M. A γ-Amino Acid That Favors 12/10-Helical Secondary Structure in $\alpha/\ \gamma$-Peptides. *Journal of American Chemical Society* **2014**, *136*, 15046–15053.

(27) Nodes, W. J.; Nutt, D. R.; Chippindale, A. M.; Cobb, A. J. A. Enantioselective Intramolecular Michael Addition of Nitronates onto Conjugated Esters: Access to Cyclic gamma-Amino Acids with up to Three Stereocenters. *Journal of the American Chemical Society* **2009**, *131*, 16016–16017.

(28) Nodes, W. J.; Shankland, K.; Rajkumar, S.; Cobb, A. J. A. Asymmetric Phase-Transfer-Catalyzed Synthesis of Five-Membered Cyclic γ-Amino Acid Precursors. *Synlett* **2010**, *2010*, 3011–3014.

(29) Al-Ani, W.; Shankland, K.; Cobb, A. J. A. Asymmetric Organocatalytic Synthesis of Cyclopentane γ-Nitroketones. *Synlett* **2016**, *27*, 17–20.

(30) Aitken, L. S.; Hammond, L. E.; Sundaram, R.; Shankland, K.; Brown, G. D.; Cobb, A. J. Asymmetric cyclopropanation of conjugated cyanosulfones using a novel

cupreine organocatalyst: Rapid access to δ 3 -amino acids. *Chemical Communications* **2015**, *51*, 13558–13561.

(31) Baxendale, I. R.; Ernst, M.; Krahnert, W.-R.; Ley, S. V. Application of Polymer-Supported Enzymes and Reagents in the Synthesis of γ-Aminobutyric Acid (GABA) Analogues. *Synlett* **2002**, *10*, 1641–1644.

(32) Cobb, A. J.; Shaw, D. M.; Ley, S. V. 5-Pyrrolidin-2-yltetrazole: A New, Catalytic, More Soluble Alternative to Proline in an Organocatalytic Asymmetric Mannich-type Reaction. *Synlett* **2004**, 558–560.

(33) Cobb, A. J. A.; Longbottom, D. A.; Shaw, D. M.; Ley, S. V. 5-Pyrrolidin-2-yltetrazole as an asymmetric organocatalyst for the addition of ketones to nitro-olefins. *Chemical Communications* **2004**, 1808–1809.

(34) Cobb, A. J. A.; Shaw, D. M.; Longbottom, D. A.; Gold, J. B.; Ley, S. V. Organocatalysis with proline derivatives: improved catalysts for the asymmetric Mannich, nitro-Michael and aldol reactions. *Organic & Biomolecular Chemistry* **2005**, *3*, 84–96.

(35) Hartikka, A.; Arvidsson, P. I. Rational design of asymmetric organocatalysts—increased reactivity and solvent scope with a tetrazolic acid. *Tetrahedron: Asymmetry* **2004**, *15*, 1831–1834.

(36) Hartikka, A.; Arvidsson, P. I. 5-(Pyrrolidine-2-yl)tetrazole: Rationale for the increased reactivity of the tetrazole analogue of proline in organocatalyzed aldol reactions. *European Journal of Organic Chemistry* **2005**, 4287–4295.

(37) Torii, H.; Nakadai, M.; Ishihara, K.; Saito, S.; Yamamoto, H. Asymmetric Direct Aldol Reaction Assisted by Water and a Proline-Derived Tetrazole Catalyst. *Angewandte Chemie International Edition* **2004**, *43*, 1983–1986.

(38) Momiyama, N.; Torii, H.; Saito, S.; Yamamoto, H. O-nitroso aldol synthesis: Catalytic enantioselective route to α-aminooxy carbonyl compounds via enamine intermediate. *Proceedings of the National Academy of Sciences* **2004**, *101*, 5374–5378.

(39) Chang, G.; Guida, W. C.; Still, W. C. An internal-coordinate Monte Carlo method for searching conformational space. *Journal of the American Chemical Society* **1989**, *111*, 4379–4386.

(40) Kolossváry, I.; Guida, W. C. Low Mode Search. An Efficient, Automated Computational Method for Conformational Analysis: Application to Cyclic and Acyclic Alkanes and Cyclic Peptides. *Journal of the American Chemical Societyl* **1996**, *118*, 5011–5019.

(41) Kolossváry, I.; Guida, W. C. Low-mode conformational search elucidated: Application to C39H80 and flexible docking of 9-deazaguanine inhibitors into PNP. *Journal of Computational Chemistry* **1999**, *20*, 1671–1684.

(42) Schrödinger Release 2017-1: MacroModel,. Schrödinger, LLC, New York, NY, 2019.

(43) Jorgensen, W. L.; Tirado-Rives, J. The OPLS [optimized potentials for liquid simulations] potential functions for proteins, energy minimizations for crystals of cyclic peptides and crambin. *Journal of the American Chemical Society* **1988**, *110*, 1657–1666.

(44) William L. Jorgensen, .; ; David S. Maxwell,; Tirado-Rives, J. Development and Testing of the OPLS All-Atom Force Field on Conformational Energetics and Properties of Organic Liquids. **1996**,

(45) Shivakumar, D.; Williams, J.; Wu, Y.; Damm, W.; Shelley, J.; Sherman, W. Prediction of Absolute Solvation Free Energies using Molecular Dynamics Free Energy Perturbation and the OPLS Force Field. *Journal of Chemical Theory and Computation* **2010**, *6*, 1509–1519.

(46) Frisch, M. J. et al. Gaussian09 Revision E.01. Gaussian Inc. Wallingford CT 2009.

(47) Chai, J.-D.; Head-Gordon, M. Long-range corrected hybrid density functionals with damped atom–atom dispersion corrections. *Physical Chemistry Chemical Physics* **2008**, *10*, 6615.

(48) Ditchfield, R.; Hehre, W. J.; Pople, J. A. Self-Consistent Molecular-Orbital Methods. IX. An Extended Gaussian-Type Basis for Molecular-Orbital Studies of Organic Molecules. *The Journal of Chemical Physics* **1971**, *54*, 724–728.

(49) Hehre, W. J.; Ditchfield, R.; Pople, J. A. Self—Consistent Molecular Orbital Methods. XII. Further Extensions of Gaussian—Type Basis Sets for Use in Molecular Orbital Studies of Organic Molecules. *The Journal of Chemical Physics* **1972**, *56*, 2257–2261.

(50) Hariharan, P. C.; Pople, J. A. The influence of polarization functions on molecular orbital hydrogenation energies. *Theoretica Chimica Acta* **1973**, *28*, 213–222.

(51) Grimme, S. Supramolecular Binding Thermodynamics by Dispersion-Corrected Density Functional Theory. *Chemistry - A European Journal* **2012**, *18*, 9955–9964.

(52) Paton Lab,; Rodríguez-Guerra, J.; Chen, J.; IFunes, bobbypaton/GoodVibes: GoodVibes v3.0.0. 2019; `https://zenodo.org/record/3346166`.

(53) Marenich, A. V.; Cramer, C. J.; Truhlar, D. G. Universal Solvation Model Based on Solute Electron Density and on a Continuum Model of the Solvent Defined by the Bulk Dielectric Constant and Atomic Surface Tensions. *The Journal of Physical Chemistry B* **2009**, *113*, 6378–6396.

(54) Ribeiro, R. F.; Marenich, A. V.; Cramer, C. J.; Truhlar, D. G. Use of Solution-Phase Vibrational Frequencies in Continuum Models for the Free Energy of Solvation. *The Journal of Physical Chemistry B* **2011**, *115*, 14556–14562.

(55) Patora-Komisarska, K.; Benohoud, M.; Ishikawa, H.; Seebach, D.; Hayashi, Y. Organocatalyzed Michael Addition of Aldehydes to Nitro Alkenes - Generally Accepted Mechanism Revisited and Revised. *Helvetica Chimica Acta* **2011**, *94*, 719–745.

(56) Iwamura, H.; Mathew, S. P.; Blackmond, D. G. In-situ Catalyst Improvement in the Proline-Mediated α-Amination of Aldehydes. *Journal of American Chemical Society* **2004**, *126*, 11770–11771.

(57) Iwamura, H.; Wells, D. H.; Mathew, S. P.; Klussmann, M.; Armstrong, A.; Blackmond, D. G. Probing the Active Catalyst in Product-Accelerated Proline-Mediated Reactions. *Journal of the American Chemical Society* **2004**, *126*, 16312–16313.

(58) Burés, J.; Armstrong, A.; Blackmond, D. G. Curtin-Hammett Paradigm for Stereocontrol in Organocatalysis by Diarylprolinol Ether Catalysts. *Journal of the American Chemical Society* **2012**, *134*, 6741–6750.

(59) Burés, J.; Armstrong, A.; Blackmond, D. G. Correction to Curtin-Hammett Paradigm for Stereocontrol in Organocatalysis by Diarylprolinol Ether Catalysts. *Journal of the American Chemical Society* **2012**, *134*, 14264.

(60) Duschmalé, J.; Wiest, J.; Wiesner, M.; Wennemers, H. Effects of internal and external carboxylic acids on the reaction pathway of organocatalytic 1,4-addition reactions between aldehydes and nitroolefins. *Chemical Science* **2013**, *4*, 1312–1318.

(61) Sahoo, G.; Rahaman, H.; Madarász, Á.; Pápai, I.; Melarto, M.; Valkonen, A.; Pihko, P. M. Dihydrooxazine Oxides as Key Intermediates in Organocatalytic Michael Additions of Aldehydes to Nitroalkenes. *Angewandte Chemie International Edition* **2012**, *51*, 13144–13148.

(62) Földes, T.; Madaraz, A.; Revesz, A.; Dobi, Z.; Varga, S.; Hamza, A.; Nagy, P.; Pihko, P. M.; Papai, I. Stereocontrol in Diphenylprolinol Silyl Ether Catalyzed Michael

Additions: Steric Shielding or CurtinHammett Scenario? *Journal of the American Chemical Society* **2017**, *139*, 17052–17063.

(63) Vasudev, P.; Chatterjee, S.; Ananda, K.; Shamala, N.; Balaram, P. Hybrid $\alpha\gamma$ Polypeptides: Structural Characterization of a C_{12}/C_{10} Helix with Alternating Hydrogen-Bond Polarity. *Angewandte Chemie International Edition* **2008**, *47*, 6430–6432.

(64) Vasudev, P. G.; Chatterjee, S.; Narayanaswamy, S.; Padmanabhan, B. Structural chemistry of peptides containing backbone expanded amino acid residues: Conformational features of β, γ, and hybrid peptides. *Chemical Reviews* **2011**, *111*, 657–687.

(65) Sharma, G. V. M.; Jadhav, V. B.; Ramakrishna, K. V. S.; Jayaprakash, P.; Narsimulu, K.; Subash, V.; Kunwar, A. C. 12/10-and 11/13-Mixed Helices in α/γ-and β/γ-Hybrid Peptides Containing C-Linked Carbo-γ-amino Acids with Alternating α- and β-Amino Acids. *Journal of the American Chemical Society* **2006**, *128*, 14657–14668.

Graphical TOC Entry